Plasma Structure Inside and Outside a Helicon Thruster

J. Navarro, M. Merino and E. Ahedo

Plasmas and Space Propulsion Team, Universidad Politécnica de Madrid

A helicon thruster consists of a cylindrical helicon source, where the plasma is generated and heated, and a magnetic nozzle, where the plasma beam is accelerated supersonically. Two dimensional models of the plasma flow inside the source and in the external magnetic nozzle (MN) are derived, for a known amount of absorbed power from rf waves. 2D plasma structure and response inside the source are described, comprising the processes of neutral depletion, losses to chamber walls, and backward and forward flows. Conditions for high propellant utilization and high current efficiency are determined. The matching with the MN model allows to obtain an overall characterization of helicon thruster performances in terms of power, thrust and efficiency.

Helicon Thruster Sketch

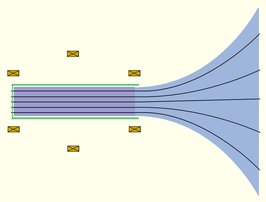

A Maxwell coil produces an almost constant ($\nabla|\mathbf{B}| \sim 0$), axial magnetic field along the dielectric tube, that diverges smoothly downstream, forming a MN. The dielectric tube, depicted in light green, isolates electrically the plasma. Two regions are distinguished: *(i)* The source domain purple coloured, is delimited by both, dielectric walls (A and W), and the tube exit section, E. *(ii)* The MN, blue coloured, matches the source at E and extends until a conductive plate, P. MN edge $R_v(z)$ is determined by the magnetic field shape. The downstream plate is needed to perform a global balance of the complete device. Electrostatic sheaths AB, QW, DP are attached to the walls. Independent models are formulated for source and nozzle.

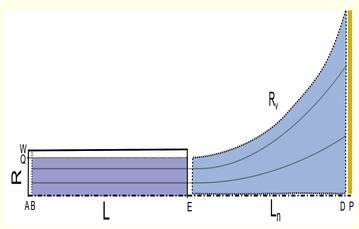

Helicon Source: Plasma Model & Hypotheses

Plasma dynamics inside the source is driven by continuity and plasma momentum equations:

$$\nabla\cdot(n_e\mathbf{u_e}) = \nabla\cdot(n_i\mathbf{u_i}) = -\nabla\cdot(n_n\mathbf{u_n}) = n_e n_n R_{ion}$$

$$\nabla\cdot(m_j n_j \mathbf{u_j}\mathbf{u_j}) = -\nabla T_j n_j - q_j n\nabla\phi + q_j n_j \mathbf{u_j}\times\mathbf{B} - \mathbf{S_j}$$

n for densities, $\mathbf{u}$ for velocities, T for temperatures, m and q species mass and charge, ϕ the electric potential, R for ionization/collision rates, $\mathbf{S}$ includes momentum sources/sinks terms. Subscript j = ion, electron, neutral.

Hypotheses:

✓ Quasineutral plasma $n_e = n_i$ delimited by B and Q.

✓ Zero-beta limit → negligible induced magnetic field.

✓ Isothermal plasma with $T_e >> T_i, T_n$.

✓ Axial symmetry $\partial/\partial\theta = 0$.

✓ Cold neutrals, $\mathbf{u}_n = u_n\mathbf{1}_z$ and $n_n(r,z) = n_n(z)$.

✓ Current ambipolarity $\mathbf{j} - j_\theta\mathbf{1}_\theta = \mathbf{0}$.

✓ Decoupled density, $n(z,r) = n_z(z)n_r(z,r)$, with $\int_0^R rn_r(z,r)dr = R^2/2$.

✓ Decoupled electric potential, $\phi(z,r) = \phi_z(z) + \phi_r(z,r)$.

✓ Ion pressure negligible compared with electron pressure.

✓ $u_{\theta i} \ll u_{\theta e} \equiv u_\theta$

✓ Spatial gradients satisfy: $\partial\chi/\partial z \ll \partial\chi/\partial r$ for $\chi = n_r, \phi_r, u_r, u_\theta, u_z$.

These hypotheses reduce the 2D problem into radial and axial models coupled through the wall recombination function, $S_w(z) \equiv n_z\nu_w(z)$.

Axial equations

After manipulating main equations, using properly all hypotheses, the set of equations that control the axial behaviour of the plasma along the dielectric tube becomes:

$$n_z u_z + n_n u_n = g_0$$

$$(c_s^2 - u_z^2)\frac{\partial u_z}{\partial z} = (u_z - u_n)u_z n_n(R_{in} + R_{ion}) + c_s^2(n_n R_{ion} - \nu_w)$$

$$(c_s^2 - u_z^2)\frac{\partial n_z}{\partial z} = -n_z\left[u_z\left(n_n R_{ion} - \nu_w\right) - \left(u_z - u_n\right)n_n\left(R_{in} + R_{ion}\right)\right]$$

$$n_n u_n\frac{\partial u_n}{\partial z} = n_z\left[u_n\nu_w\left(\alpha_w - 1\right) + \left(u_z - u_n\right)n_n R_{in}\right]$$

g_0 the mass flux, $c_s = \sqrt{T_e/m_i}$ the sonic velocity, α_w is an adjustable parameter that retains the momentum loss/gain due to recombination at the lateral wall.

Boundary conditions: $u_{zB} = -c_s, \quad u_{zE} = c_s, \quad u_{nB} = u_{n0}, \quad g_0$ known.

The plasma axial response depends on four dimensionless parameters:

$$L_* = c_s u_{n0}/R_{ion}g_0, \qquad R_{in}/R_{ion}, \qquad u_{n0}/c_s, \qquad \alpha_w.$$

(ν_w is obtained self-consistently solving the radial model)

Analytical solution is found invoking asymptotic limits, high-confinement $\nu_w/n_n R_{ion} \ll 1$ and $R_{in}/R_{ion} < u_{n0}/c_s \ll 1$,

$$u_n = u_{n0}, \qquad \frac{u_z}{c_s} = \tan\xi, \qquad \frac{c_s}{g_0}n_z = 2\eta_u\cos^2\xi, \qquad \frac{u_{n0}}{g_0}n_n = 1 - \eta_u\sin 2\xi,$$

$$\frac{z}{L_\star} = \int_{-\pi/4}^{\xi}\frac{1-\tan^2\xi'}{1-\eta_u\sin 2\xi'}d\xi', \ \eta_u \text{ is the propellant utilization from } z(\pi/4) = L.$$

Radial Equations

The radial model was treated in Ref. [3], main equations are listed next. ν_w is the eigenvalue that assures the correct plasma flow balance.

$$\frac{1}{r}\frac{\partial}{\partial r}(rn_r u_r) = n_r\nu_w$$

$$u_r\frac{\partial u_r}{\partial r} = -c_s^2\frac{\partial \ln n_r}{\partial r} - \frac{eB}{m_i}u_\theta + \frac{m_e}{m_i}\frac{u_\theta^2}{r} - n_n\left(R_{in} + R_{ion}\right)u_r$$

$$u_r\frac{\partial u_\theta}{\partial r} = \frac{eB}{m_e}u_r - \left[n_n(R_{en} + R_{ion}) + nR_{ei}\right]u_\theta - \frac{u_\theta u_r}{r}$$

$$e\frac{\partial\phi_r}{\partial r} = T_e\frac{\partial \ln n_r}{\partial r} + eBu_\theta - m_e\frac{u_\theta^2}{r}$$

Matching with the MN Model

The source model matches the 2D MN model of Ahedo and Merino Ref. [4]. It provides the supersonic plasma expansion. Currents developed at the plasma plume are closed at P, where $\phi_P = const$. This potential is solved mixing fluid-kinetic formulation at the sheath transition D.

MN Hypotheses:

✓ Isothermal, quasi-neutral plasma expansion.

✓ Collisionless.

✓ Fully-magnetized electrons and partially-magnetized ions.

✓ Current free plasma.

✓ No current ambipolarity.

Axial Response

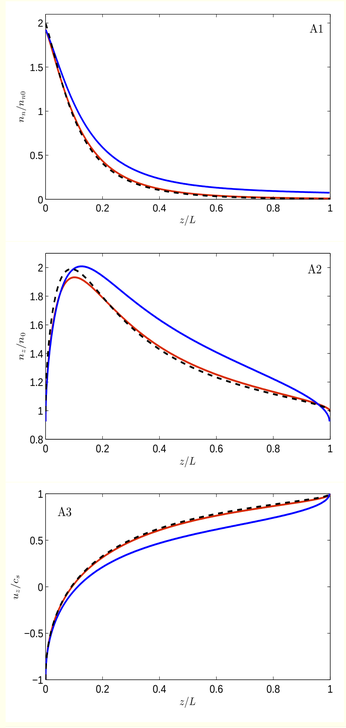

⋆ **Case 1 (200G)** ⋆ **Case 2 (600G)** ⋆ **Analytical solution, dashed line.**

✓ All other parameters: $T_e = 10\,eV$, $\dot{m} = 0.1\,mg/s$, $\alpha_w = 1.0$, $u_{n0} = 350\,m/s$ remain constant. *Neutral depletion* (Fig. A1) is governed by plasma ionization, $\nu_{ion} \propto n_n R_{ion}(T_e)$, and wall recombination ν_w. Higher temperatures and magnetic fields, and longer tubes improve the propellant utilization η_u.

✓ Plasma density (Fig. A2) presents a peak near $u_z \sim 0$ (Fig. A3). The positive gradient of this magnitude close to B is due to ionization. $\partial_z n_z < 0$ in the forward flow region is related to the plasma acceleration.

✓ Case 2 solution is almost indistinguishable from the analytical one because plasma parameters agree with asymptotic limit hypotheses. Otherwise, case 1 shows the role of wall losses ν_w on the plasma axial dynamics (Fig. A4), resulting a worse correlation with the ideal-analytical solution.

✓ Effective electron collisions (Fig. A5), governing radial dynamics, decrease along the chamber, thus increasing radial magnetic confinement. Note also that $\nu_e \sim \nu_{en}(z)$ near B and $\nu_e \sim \nu_{ei}(z,r)$ near E.

Radial Response

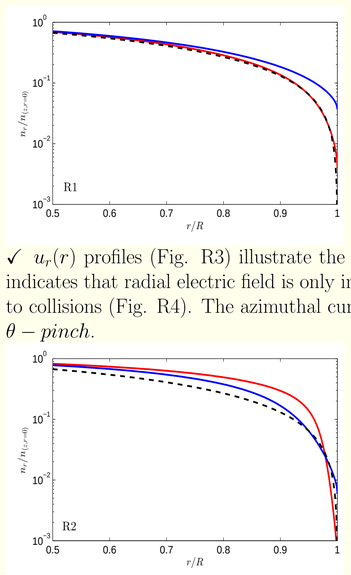

✓ Fig. R1 depicts plasma density profiles at the rear section B. There, case 2 is in agreement with the asymptotic solution proposed by Ref. [3], because both $\omega_{lh} = eB/\sqrt{m_e m_i} \gg \nu_e$ (high-magnetized plasma) and $\nu_e(z,r) \sim \nu_{en}(z)$ (radially-constant collisions). Case 1 does not fulfil the analytical solution because $\omega_{lh} \sim \nu_e$. Fig. R2 refers to section E, where $\nu_e(r) \sim \nu_{ei}(r) \propto n_r$ makes these profiles more steepened.

Analytical solution: $n_r(z,r) = n_r(z,0)J_0\left(a_0 r/R\right)$

where a_0 is the first 0 of Bessel function, J_0.

✓ $u_r(r)$ profiles (Fig. R3) illustrate the high magnetic confinement. Taking into account that $-e\phi \sim m_i u_r^2/2$, last result indicates that radial electric field is only important in a thin inertial layer preceding the Debye sheath. $u_\theta(r)$ develops thanks to collisions (Fig. R4). The azimuthal current provides the magnetic force that sustains the large radial density drop as in a $\theta - pinch$.

2D Maps

Source details: Case 1 results are presented below for the plasma density and velocity. Large gradients of these magnitudes appear close to all walls. Radial gradients increase with magnetic confinement, in fact with the Hall parameter ω_{lh}/ν_e. Axial gradients close to A/B are due to electrostatic confinement and drive the backstreaming flow.

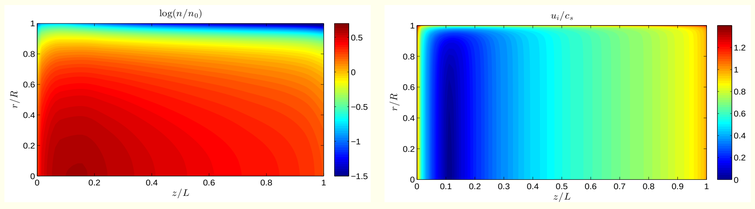

Helicon Thruster maps: The plasma density distribution along the complete device is depicted here, $\log n/n_0$, being $n_0 = g_0/c_s$. It manifests how density varies much less inside the source than in the plume, where it may drop up to 4 orders of magnitude, presenting a high *radial rarefaction*. Electric potential gradients inside the source are purely axial, because plasma is radially confined by the magnetic field. Equipotential lines become curved as advancing along the MN.

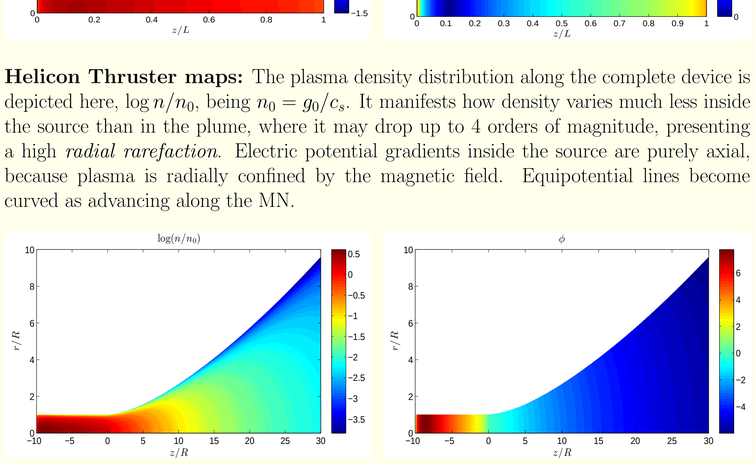

Helicon Source Performances

✓ **Propellant utilization:** $\eta_u = \dfrac{\dot{m}_{iE}}{\dot{m}}$ ✓ **Production efficiency:** $\eta_p = \dfrac{\dot{m}_{iE}}{\dot{m}_{iA} + \dot{m}_{iW} + \dot{m}_{iE}}$

✓ Analytical law for $L/L_* = f(\eta_u)$ states that η_u increases with T_e, L and $\dot{m}$, requiring $L_* > 2.5$ to obtain a high propellant utilization, $\eta_u > 0.95$ (Fig. S1).

✓ $\eta_u - B$ curves are plotted for different electron temperatures (Fig. S2). The knee of each η_u curve separates low-utilization regimes (low-magnetized plasmas) from the high-utilization regimes. Note also, even for very high magnetic field intensities, high-utilization regimes are limited by the plasma temperature, noticeable in the case $T_e = 7\,eV$, in which ionization is compensated by wall losses, limiting the maximum η_u available.

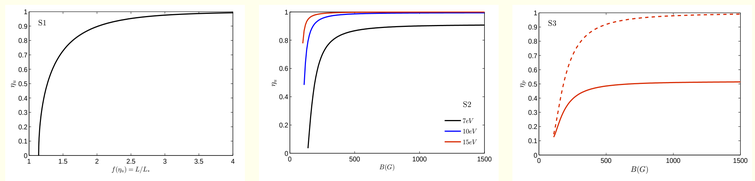

✓ The flow to the rear wall should be reduced because represents almost 50% of η_p losses (Solid red line in Fig. S3). If a perfect magnetic screening is assumed at the rear wall, η_p may reaches values over 90% for the typical range of magnetic field intensities $500 - 1000G$ (dashed red line).

✓ Curves of constant efficiencies, η_u and η_p, are depicted on the parametric plane $B - \dot{m}$ (Fig. S4). These are useful to:

✓ Optimize the helicon source efficiencies.

✓ Obtain a clear map of the region where the sensitivity to parametric deviations is smaller, here, the knee of η_u curves.

It may be predicted that operating the source close to this zone is a good choice in terms of parameter sensitivities and efficiency.

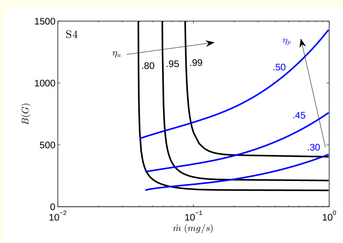

Helicon Thruster Performances

✓ **Global energy balance** determines the relation between the absorbed power, the **constant plasma temperature**, and the length L_n of the nozzle region (Fig. T1). The energy equation grouping all contributions of all species is integrated over the whole domain, yielding a relation between the power through the boundaries P_P and P_{A+W}, ionization P_{ion} and absorbed power P_a.

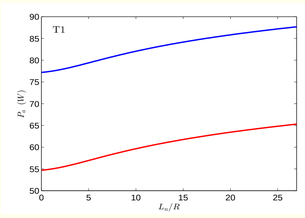

$$\nabla\cdot\dot{P} = \mathbf{j}\cdot\mathbf{E} + \dot{P}_a - \dot{P}_{ion} \quad \rightarrow \quad P_P + P_{A+W} + P_{ion} = P_a$$

✓ For T_e = const, P_a increases as MN length is extended, because P_P rises monotonically in this MN isothermal model. Reciprocally, T_e decreases for longer MN and P_a = const. At $L_n = 0$, the difference between P_a, case 1, from that obtained in case 2, responds to the lower production efficiency of the source, penalized by wall losses and ionization of the recombined flux, $P_{A+W} + P_{ion} \simeq 0.7P_a$ (Fig. T2). Case 2 is shown as an efficient case, $P_P \simeq 0.45P_a$.

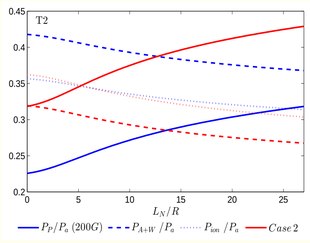

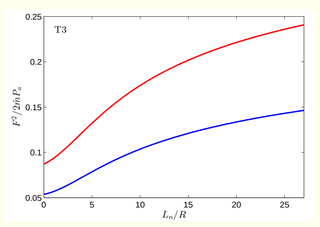

✓ **Thrust efficiency,** $F^2/2\dot{m}P_a$, is evaluated taking into account all contributions to the thrust F,

$$F = F_{pres} + F_{elec} + F_{mag}$$

Terms on the RHS retain the contribution of pressure on walls F_{pres}, electrostatic sheath at the back wall F_{clec}, and MN contribution F_{mag}. Thrust is related to plasma axial momentum flow, F_z, at sections E and D: $F_{zE} = F_{pres} + F_{elec}$ and $F_{zD} = F$. Case 2 thrust efficiency is over 20% if $L_n/R \geq 14$ (Fig. T3).

Conclusions

✓ A 2D model (Source + MN) of the helicon plasma thruster has been derived.

✓ Optimum regimes for source-related efficiencies have been determined.

✓ Analytical models are recovered at the high-magnetized regime.

✓ First model assessing global Helicon Thruster performances, including thrust efficiency and power losses.

✓ Plasma temperature depends on nozzle length.

✓ This fluiddynamic model should be coupled to plasma-wave interaction model.

✓ Main uncertainties are: power absorption, electron distribution function, radiation losses, downstream plasma detachment

References

[1] Ahedo, E., Gallardo, J. M., & Martínez-Sánchez, M. (2003). Effects of the radial-plasma wall interaction on the axial Hall thruster discharge. *Physics of Plasmas*, *10*(8), 3397-3409.

[2] Ahedo, E. (2009). Cylindrical model of a helicon-generated plasma. *31th International Electric Propulsion Conference, Ann Arbor, Michigan, USA*. IEPC 2009-193.

[3] Ahedo, E. (2009). Parametric analysis of a magnetized cylindrical plasma. *Physics of Plasmas*, *16*, 113503.

[4] Ahedo, E., & Merino, M. (2010). Two-dimensional supersonic plasma acceleration in a magnetic nozzle. *Physics of Plasmas*, *17*, 073501.

[5] Batishchev, O. V. (2009). Minihelicon Plasma Thruster. *IEEE Transaction on Plasma Science*, *37*, 1563-1571.

[6] Fruchtman, A., Makrinich, G., & Ashkenazy, J. (2005). Two-dimensional equilibrium of a low temperature magnetized plasma. *Plasma Sources Science and Technology*, *14*, 152-167.

[7] Lafleur, T., Charles, C., & Boswell, R. W. (2011). Characterization of a helicon plasma source in low diverging magnetic fields. *Journal of Physics D: Applied Physics*, *44*, 055202.

[8] Pavarin, et al. (2009). Design of 50W Helicon Plasma Thruster. *31th International Electric Propulsion Conference, Ann Arbor, Michigan, USA*. IEPC 2009-205.

[9] Slough, J., Winglee, R., & Ziemba, T. (2006). Performance enhancement and modeling of the high power helicon plasma thruster. In W. D. C. American Institute of Aeronautics and Astronautics (Ed.), *42th Joint Propulsion Conference, Sacramento, CA*. AIAA 2006-5257.

Acknowledgments

✓ Support comes from the Spanish Government (Project AYA-2010-61699) and the Air Force Office of Scientific Research, Air Force Material Command, USAF (grant FA8655-12-1-2043).

39th IEEE International Conference on Plasma Science (2P-185) Edinburgh, 8-12 July 2012

E.T.S.I. Aeronáuticos, Pza. Cardenal Cisneros 3, 28040 Madrid, Spain
http://web.fmetsia.upm.es/ep2
mailing address: eduardo.ahedo@upm.es, jaume.navarro@upm.es